Optical study of the spontaneous magnetization at marginal dimensionality

J. A. Griffin
Department of Physics, Laboratory for Research on the Structure of Matter, University of Pennsylvania, Philadelphia, Pennsylvania 19104

J. D. Litster
Department of Physics, Center for Materials Science and Engineering, Massachusetts Institute of Technology, Cambridge, Massachusetts 02139
(Received 24 May 1978)

The spontaneous magnetization in the critical region of the uniaxial, dipolar-coupled ferromagnet $LiTbF_4$ has been measured using sensitive optical techniques. The magnetic and optical properties of $LiTbF_4$ and the experimental techniques are discussed in detail. These measurements provide a quantitative comparison between the predicted logarithmic corrections to mean-field theory and the experimentally observed magnetization of a ferromagnet at marginal dimensionality. We conclude that the spontaneous magnetization in $LiTbF_4$ is described by the relation $M_c(T)/M_c(T=0) = B|t|^{1/2}|\ln|t_0/t||^{1/3}$ over the range $0.002 \leq t \leq 0.09$ with $B = 1.77 \pm 0.06$, $T_c = 2.8700 \pm 0.002$ K and $t_0 = 0.53 \pm 0.06$.

I. INTRODUCTION

As a result of recent investigations of critical phenomena, we have come to realize the vital role played by spatial dimensionality in phase transitions. Each order-disorder phase transition is characterized by both an upper and a lower marginal dimensionality. The upper marginal dimensionality d^* separates classical (mean-field theory) critical phenomena from nonclassical behavior; if the spatial dimensionality is less than the lower marginal dimensionality long-range order is not possible. Whether a system will exhibit classical critical behavior, nonclassical critical behavior, or no long-range order depends upon the influence of fluctuations in the order parameter. This influence, in turn, depends upon the phase space available to the fluctuations, hence the importance of spatial dimensionality. The importance of fluctuations arises straightforwardly when statistical-mechanical calculations are carried out by the renormalization-group method, but one can calculate d^* more simply by applying the Ginzburg criterion.[1] This has been shown very elegantly in a recent article by Als-Nielsen and Birgeneau.[2]

In this paper we present the results and analysis of an experimental study of the spontaneous magnetization of the dipolar Ising ferromagnet $LiTbF_4$, whose upper marginal dimensionality is $d^* = 3$. The results presented here were obtained by measurements of the temperature and magnetic-field dependence of the intensity of light scattered by uniaxial ferromagnetic domains in the ordered phase. The data are quantitatively compared to the logarithmic corrections to classical critical behavior that are predicted to occur at $d = d^*$, and to a simple asymptotic power-law dependence of the spontaneous magnetization. Our analysis indicates that the data experimentally confirm the occurrence of logarithmic corrections.

This paper is organized as follows. Section II discusses critical phenomena at $d = d^*$, following which we discuss the experimental technique in Sec. III. The crystal and magnetic properties of $LiTbF_4$ are reviewed in Sec. IV. The optical and magneto-optical properties are discussed in Sec. V, where we also present the experimental results. These are analyzed in Sec. VI, and we compare them with the results of other experiments and present our conclusions in Sec. VII.

II. THEORY

Our understanding of phase transitions and critical phenomena has been placed on a much sounder theoretical basis by the application of the renormalization-group technique to statistical mechanics.[3] As a result, we have quantitative predictions for nonclassical critical behavior of systems when the spatial dimensionality d is lower than the marginal dimensionality d^*. The critical-point exponents are expressed in a perturbation expansion in the parameter $\epsilon = d^* - d$, and the expansion coefficients depend upon the order parameter dimensionality n. Thus, for example, in the n-vector model one obtains,[4] for

the susceptibility exponent,

$$\gamma = \gamma_{\mathrm{MFT}} + \frac{n+2}{2(n+8)}\epsilon + \frac{(n+2)(n^2+22n+52)}{4(n+8)^3}\epsilon^2 + \cdots , \quad (1)$$

where $\gamma_{\mathrm{MFT}} = 1$. It is not always known how well these expansions converge, and so for most isotropic systems with $d^* = 4$, the renormalization-group predictions are necessarily approximate. For $n = 1$ and $\epsilon = 1$ (three-dimensional Ising model), the results are $\gamma = 1.17$ to $O(\epsilon)$, 1.24 to $O(\epsilon^2)$, and 1.19 to $O(\epsilon^3)$; in lower-dimensional systems the ϵ-expansion results will be even less certain.

A central result of the renormalization-group approach is that the equations can be solved "exactly," without ϵ or $1/n$ expansions, when $d = d^*$. The prediction then is for logarithmic corrections to the mean-field results[5]; thus experiments at the upper marginal dimensionality can provide a stringent test of the renormalization-group calculations.

The marginal dimensionality d^* depends on the type of critical point. In magnetic materials there are only four known values of d^*. In short-range exchanged-coupled magnetic systems, $d^* = 4$. In the percolation transition, which is geometrically driven rather than thermally driven, $d^* = 6$. In tricritical phenomena, $d^* = 3$, and in three-dimensional dipolar-coupled Ising ferromagnets, $d^* = 3$. As a result of these values of d^*, it is only possible to expect to experimentally observe marginal dimensionality in magnetic cooperative phenomena in the last two cases. Marginal dimensionality at $d = 3$ occurs at tricritical points due to the interplay of two types of order parameters, whereas in the last example it occurs as a special property of the dipolar interaction in Ising systems.

Magnetic dipole-dipole interactions are present in all real magnetic materials. In most magnetic materials this long-range interaction is much weaker than the short-range exchange forces, and in the initial renormalization-group calculations, such dipolar forces were ignored. Aharony[6] considered the effect of dipolar forces on the critical behavior of various magnetic systems. In the case of systems with $n = 2$ and $n = 3$, Aharony found that the dipolar interactions drive the critical point to a new renormalization-group fixed point with new critical-point exponents, but the numerical difference in these two sets of exponents amounts only to approximately 10%. Moreover, the temperature at which crossover to the new fixed point is expected to occur is quite close to the phase transition. Thus the effect of dipolar interactions on these systems is not spectacular and is difficult to measure quantitatively. But when $n = 1$, the dipolar interaction dramatically influences the critical behavior and reduces the marginal dimensionality to $d^* = 3$.

The reason for this can be seen by means of the Ginzburg criterion for the importance of fluctuations. One simply compares the relative magnitude of the order parameter $\langle M \rangle$ with the root-mean-squared fluctuations $\langle \delta M^2 \rangle_p^{1/2}$ at a point in the magnet. If $\langle \delta M^2 \rangle_p$ exceeds $\langle M \rangle^2$ near T_c, the mean-field approximation will fail. The mean-field result predicts $\langle M \rangle^2 \sim T_c - T$. The magnetization is an intensive variable, thus the fluctuations in a volume V are $\langle \delta M^2 \rangle_V \sim kT\chi/V$, where the susceptibility χ varies as $(T_c - T)^{-1}$. To calculate the fluctuations at a point, one replaces V by ξ^d in a d-dimensional isotropic magnet. Since the correlation length diverges as $(T_c - T)^{-1/2}$, we expect to find the following:

$$\langle \delta M^2 \rangle_p / \langle M \rangle^2 \sim |T_c - T|^{(d-4)/2} . \quad (2)$$

This shows that the mean-field approximation holds for $d > 4$ and thus $d^* = 4$.

In the Ising system where dipolar interactions dominate, the wave-vector dependent susceptibility at long wavelengths has the rather unusual form[6] shown here:

$$\chi(T, \vec{q}) = \chi(T, 0)[1 + \xi^2 q^2 + g\xi^2(q_z^2/q^2) - b\xi^2 q_z^2] , \quad (3a)$$

where g and b are functions of the dipolar coupling and the exchange coupling. The correlation function for fluctuations δM is the Fourier transform of $\chi(T, \vec{q})$; thus the correlation volume grows as ξ^2 along the z axis and ξ in other directions. Accordingly, we have

$$\langle \delta M^2 \rangle_p / \langle M \rangle^2 \sim |T_c - T|^{(d-3)/2} , \quad (3b)$$

and the marginal dimensionality is $d^* = 3$.

Aharony and Halperin calculated[7] the critical behavior predicted in the $n = 1, d = 3$ dipolar-coupled Ising ferromagnet. The behavior is identical to that of a uniaxial ferroelectric.[8] The normalized spontaneous magnetization $M_c(T)/M_c(0)$ is described by the equation

$$\frac{M_c(T)}{M_c(0)} = B|t|^{1/2}|\ln t|^{1/3}(1 + \cdots) , \quad (4)$$

where the mean-field result

$$M_c(T)/M_c(0) = Bt^{1/2} \quad (5)$$

is corrected by the logarithmic factors. Here $(1 + \cdots)$ represents higher-order logarithmic corrections, $M_c(0)$ is the zero-temperature saturation magnetization, $t = (T_c - T)/T_c$ is the reduced temperature, and B is an amplitude coefficient. The nonclassical power law normally found to describe magnetic-phase transitions is

$$M_c(T)/M_c(T = 0) = Bt^{\beta} , \quad (6)$$

where $\beta(n=1,d=3)\simeq 0.33$ if dipolar forces are not present. Other quantities calculated by Aharony and Halperin are

$$C_H = A\,|\ln t|^{1/3}(1+\cdots)\ , \tag{7}$$

$$\chi = \Gamma |t|^{-1}|\ln t|^{1/3}(1+\cdots)\ , \tag{8}$$

and the relation

$$\xi^2\xi_{\parallel}C_H t^2/\left|\ln|t|\,\right| = 3k_B/32\pi\ , \tag{9}$$

where $\xi_{\parallel}=g\xi^2$ is an effective longitudinal correlation length, and k_B is Boltzmann's constant. To first order in $(1+\cdots)$, the higher-order correction is the same in the expressions for χ and C_H. It is the purpose of the experiment described in this paper to experimentally test the prediction of Eq. (4).

III. EXPERIMENTAL

The experimental objective in this work is to determine the temperature dependence of the spontaneous magnetization in $LiTbF_4$ near T_c. Moreover, the measurements are intended to detect the presence or absence of logarithmic factors in the power-law behavior of the magnetization. Due to the small numerical difference between the two possible theoretical descriptions, the magnetization must be determined with considerable accuracy over a large range in reduced temperature. The difficulty in such measurements is not in the measurement of the magnetization, but is in the location, in the M, $H_{\rm ext}$, T space, of the ferromagnetic-paramagnetic coexistence curve. In order to accurately determine the position of the ferromagnetic-paramagnetic phase boundary, light scattering from ferromagnetic domains was used.

A. Optical technique

The measurements presented here consist of a determination of the external magnetic field and temperature dependence of the onset of domain diffraction. This onset of diffraction is used as an optical indicator of the location of the paramagnetic-ferromagnetic coexistence curve. In order to make measurements of this phase boundary with sufficient resolution, a two-beam optical-bridge system was constructed using polarization modulation techniques. In this manner, the transmitted intensity in the paramagnetic phase, which is quite large as a result of the transparency of the crystal of $\lambda = 6328$ Å, can be nulled, and small changes in scattering that occur at the paramagnetic-ferromagnetic boundary can then be detected with higher resolution. The details of this optical bridge are described in the Appendix, and Fig. 1 illustrates the bridge schematically.

B. Cryogenics and sample holders

The optical cryostat used in this experiment was a Janis Cryogenics varitemp $6DT$ cryostat with optical access. The sample holder was positioned in an exchange-gas tube surrounded on the outside by pumped liquid helium, apart from the optical path, and filled in the inside with approximately 25 μ of ^{4}He exchange gas. The crystal was mounted on an oxygen-free high-conductivity copper (OFHC) sample holder with small amounts of vacuum grease to insure thermal conductivity between the sample and the sample holder. The sample holder was thermally anchored to the 1.2-K helium bath via the exchange gas, and it was equipped with an electrical heater to raise the temperature above the helium bath. The laser-beam size was approximately 0.3 cm in diameter, and the incident intensity was approximately 10 μW. Windows at 1.2 K shielded the central part of the crystal through which the laser passed from the 77-K and 300-K radiation.

The thermometry used in this experiment consisted of a calibrated Ge resistance thermometer and an uncalibrated capacitance thermometer for temperature

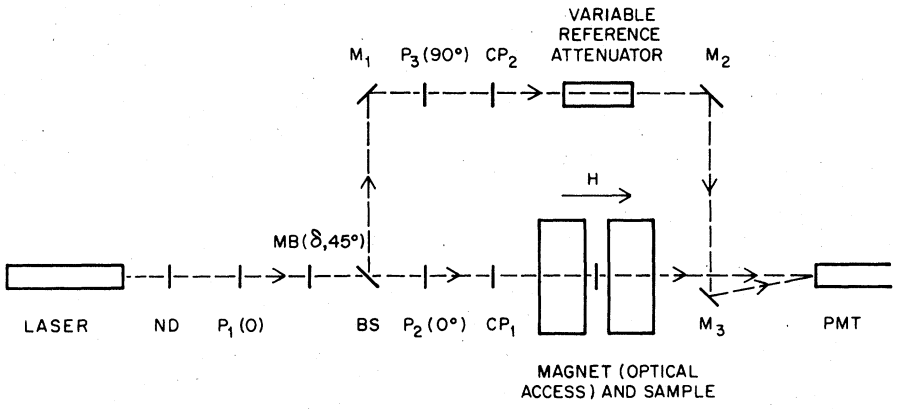

FIG. 1. Schematic diagram of the double-beam optical bridge used to detect the ferromagnetic domain scattering. The operation of this bridge is described in the Appendix.

control. In order to avoid the problems of calibration repeatability in the Ge thermometer that occur upon room-temperature cycling, the liquid-^{4}He level in the cryostat was maintained throughout the duration of the experiment, thereby not allowing the sample holder to exceed 4.2 K. The temperature control was obtained by use of the magnetic-field independent strontium titanate capacitance thermometer and an ac bridge capacitance controller. The stability of the temperature was measured by an independent ac resistance bridge using the Ge thermometer. The temperature stabilities listed in Table I were obtained by recording the Ge thermometer temperature in zero magnetic field before and after each field scan. These drifts are probably due to the drift on the capacitance sensor, which in the pumped helium temperature range is quite small. In the temperature range between 2.85 K $\leq T \leq T_c$, the temperature scans at constant magnetic field were obtained by using the capacitance thermometer controller to calibrate the germanium thermometer in a magentic field. The calibration was accomplished by measuring the temperature using the Ge thermometer in zero magnetic field with the capacitance sensor controlling the temperature. After ascertaining that the temperature had stabilized, the desired magnetic field was applied, thereby causing the Ge thermometer to indicate a new value (due to magnetoresistance) at the same temperature. This type of calibration was repeated several times for each data point in the range 2.85 K $\leq T \leq T_c$. The accuracy of this calibration was verified by the overlap of data points obtained by temperature scans at constant magnetic field with other data points obtained by field scans at constant temperature.

C. Magnet

The magnet used in these measurements was a Magnion L-128 with an FFC-4 power supply. The twelve-inch diameter pole faces had a four-inch gap between them and had $\frac{1}{4}$-in. holes drilled in them to provide optical access parallel to the magnetic field; these holes served to define a narrow forward-direction acceptance angle for the diffraction effects. The uncertainty in the external magnetic field, measured by a rotating coil Gaussmeter, was about ±1 G.

D. Crystal growth

The crystal used in these measurements was $1 \times 1 \times 0.4$ cm, with the c axis parallel to the 0.4-cm thickness. This crystal was grown by Gabbe, and the details of the technique appear in a separate publication.[9]

TABLE I. Phase-boundary field (proportional to the saturation magnetization) as a function of temperature for $LiTbF_4$.

H_c (kG)	T (k)
1.250 ± 0.140	2.8643 ± 0.0016
1.500 ± 0.123	2.8642 ± 0.0016
1.569 ± 0.121	2.8649 ± 0.0003
1.580 ± 0.178	2.8622 ± 0.0022
1.660 ± 0.127	2.8616 ± 0.0016
1.750 ± 0.131	2.8620 ± 0.0015
1.830 ± 0.120	2.8602 ± 0.0016
1.910 ± 0.090	2.8589 ± 0.0013
2.000 ± 0.203	2.8574 ± 0.0032
2.250 ± 0.064	2.8530 ± 0.0012
2.375 ± 0.036	2.8502 ± 0.0007
2.500 ± 0.037	2.8488 ± 0.0008
2.750 ± 0.033	2.8435 ± 0.0008
2.775 ± 0.120	2.8408 ± 0.0003
3.000 ± 0.025	2.8371 ± 0.0007
3.016 ± 0.120	2.8358 ± 0.0006
3.250 ± 0.030	2.8306 ± 0.0009
2.500 ± 0.014	2.8213 ± 0.0005
3.525 ± 0.048	2.8222 ± 0.0006
3.692 ± 0.024	2.8155 ± 0.0003
3.750 ± 0.021	2.8131 ± 0.0008
3.829 ± 0.019	2.8101 ± 0.0003
3.977 ± 0.025	2.8050 ± 0.0003
4.000 ± 0.017	2.8032 ± 0.0007
4.072 ± 0.024	2.8002 ± 0.0003
4.250 ± 0.024	2.7911 ± 0.0005
4.455 ± 0.024	2.7829 ± 0.0006
4.500 ± 0.012	2.7789 ± 0.0011
4.741 ± 0.025	2.7655 ± 0.0003
4.750 ± 0.011	2.7650 ± 0.0006
4.979 ± 0.024	2.7499 ± 0.0003
5.000 ± 0.012	2.7493 ± 0.0007
5.687 ± 0.023	2.6988 ± 0.0003
6.195 ± 0.023	2.6504 ± 0.0003
6.491 ± 0.011	2.6152 ± 0.0003
6.641 ± 0.025	2.6009 ± 0.0003

IV. STRUCTURAL AND MAGNETIC PROPERTIES OF $LiTbF_4$

$LiTbF_4$ is colorless and optically uniaxial. It has the same crystal structure as mineral scheelite $CaWO_4$. The space group is C_{4h}^6-$I4_1/a$, with a body-centered tetragonal unit cell with $a_\phi = 5.20$ Å and $c_\phi = 10.90$ Å. There are four Tb^{3+} ions per unit cell, each having site symmetry S_4 with the local 4 axes

parallel to [001]. Figure 2 is an illustration of this structure.

The crystal field in $LiTbF_4$ has been studied by Holmes *et al.*[10] and Hansen *et al.*[11] The atomic configuration of Tb^{3+} is $4f^8$, which has a Hund's-rule ground term of ^7F. This is then subject to perturbations from the spin-orbit coupling and crystal field. The stronger spin-orbit coupling splits the ^7F term into $^7F_6, ^7F_5, \ldots, ^7F_0$, with $^7F_6$ having the lowest energy. The S_4 symmetry crystal field then further splits each of these levels. S_4 splits the $^7F_6$ into ten levels, three E doublets comprising $J_z = \pm 5, \pm 1, \pm 3$, three A singlets comprising $J_z = 0, \pm 4$, and four B singlets comprising $J_z = \pm 6, \pm 2$. Inelastic-neutron-scattering and magnetic-susceptibility measurements have been made on $LiTbF_4$, and the resultant crystal-field splitting of the $^7F_6$ level is illustrated in Fig. 3. The Ising behavior of $LiTbF_4$ results from the two nearly degenerate B levels separated from the next levels by ~ 125 K. This isolated doublet produces an effective $S = \frac{1}{2}$, whose easy axis is the tetragonal c axis. The two B levels are each primarily $|J_z = \pm 6\rangle$ levels, but a small admixture of $|J_z = \frac{1}{2}\rangle$ occurs. This admixture produces a zero-field splitting between the two B levels. Assuming only $|J_z = \pm 6\rangle$ levels, the calculated magnetic moment μ_1 is 8.87 μ_B, compared to the experimental value[10] of 8.90 ± 0.03. The g factors are[10] $g_{\parallel} = 17.8$ and $g_{\perp} = 0.0$.

The magnetic structure of $LiTbF_4$ has also been studied by Hansen *et al.*[11] and Holmes *et al.*[10] This material orders in a three-dimensional ferromagnetic array at $T_c = 2.87$ K, with an Ising anisotropy parallel to the tetragonal c axis of the crystal field. This anisotropy produces, in the ordered phase, an array of cylindrical-like ferromagnetic domains aligned parallel and antiparallel to the tetragonal c axis. The dominant magnetic coupling responsible for this ordering is dipole-dipole coupling between Tb^{3+} ions, rather than the usual short-range exchange coupling. The neutron scattering work of Als-Nielsen *et al.*[10] has shown the following:

$$\frac{J_1}{D_1} = -0.24 \pm 0.10 , \quad \frac{J_2}{D_2} = -0.07 \pm 0.15 , \qquad (10)$$

where J_n and D_n are the exchange and dipolar coupling between the nth nearest neighbors, respectively. The relatively small exchange coupling could result from either small exchange interaction or a cancellation of exchange forces, and it is not known which, if either, is the case in $LiTbF_4$.

V. OPTICAL PROPERTIES OF $LiTbF_4$

One of the most interesting features of $LiTbF_4$ is its optical and magneto-optical behavior. These topics have been discussed by Griffin *et al.*[12] Figure 4 illustrates the absorption and Faraday rotation spectrum between 1.8 μ and 2000 Å. In this material there is a "window" of high transparency that extends from 1.6 μ to 4000 Å, and on both sides of this window strong absorption bands occur. The optical transitions present in Fig. 4 occur in the Tb^{3+} ions. In the infrared the transitions starting at 1.6 μ are between the $^7F_6$ ground term and the other $^7F_0, ^7F_1, \ldots$ levels. In the visible region there is only a single, narrow transition at 4900 Å that occurs between the ^7F and ^5D levels of the $4f^8$ ground term. In the ultraviolet, transitions are numerous, and

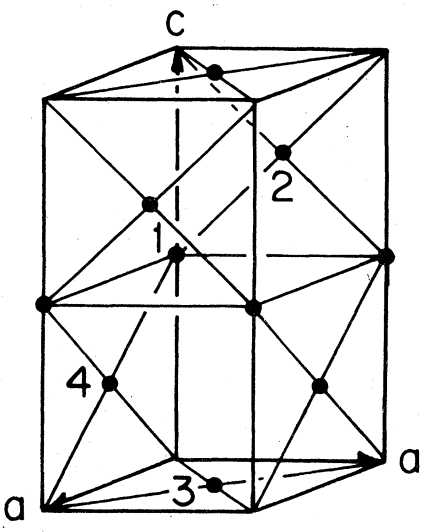

FIG. 2. Tb^{3+} positions in the body-centered tetragonal and cell of $LiTbF_4$ (from Ref. 7).

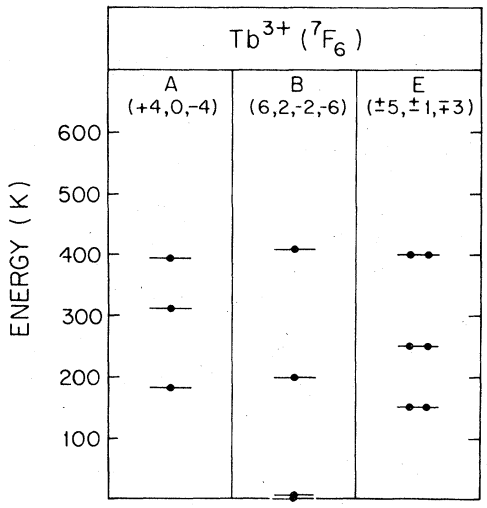

FIG. 3. Crystal-field levels of Tb^{3+} ($^7F_6$) in $LiTbF_4$.

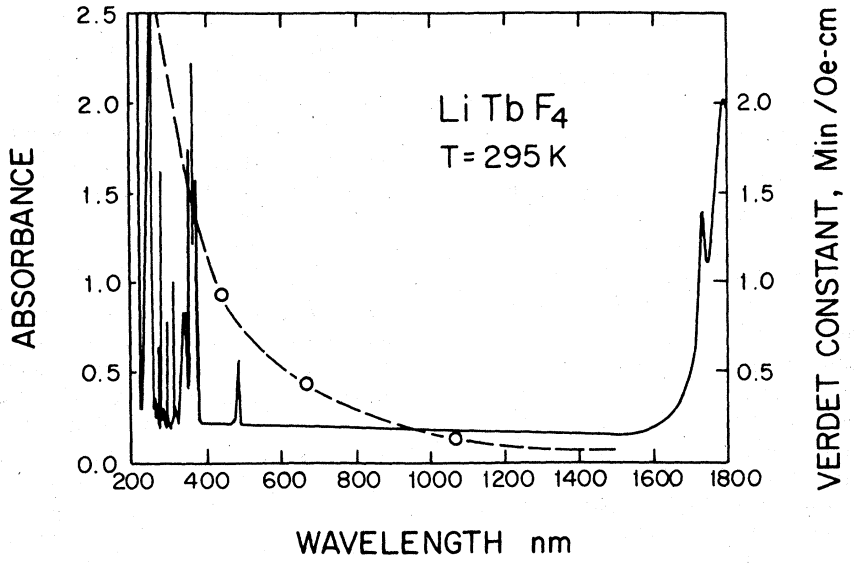

FIG. 4. Absorption and Verdet-constant spectra in $LiTbF_4$ at $T = 295$ K (from Ref. 12).

these transitions occur between the $4f^8$ and $4f^7 5d$ terms.

In spite of the high transparency in the visible-wavelength region, $LiTbF_4$ exhibits a large Faraday rotation.[12] The source of this large rotation is primarily the strong absorption bands that occur in the uv. Figure 5 illustrates the magnetic-field dependence of this rotation of $\lambda = 6328$ Å for four temperatures.[13] At high temperatures, the high transparency and simultaneous large Verdet constant (1.28×10^{-4} rad cm^{-1} Oe^{-1} at 300 K) makes $LiTbF_4$ particularly suitable as an optical modulator or optical isolator. At low temperatures Fig. 5 illustrates the proportionality between the Faraday rotation and the ground-state magnetization. At temperatures $T << T_c$, the ferromagnetic-paramagnetic phase boundary is located by the "kink" in the Faraday rotation, but near T_c such a "kink" becomes sufficiently smooth that precise determination of the phase boundary is not possible. For this reason the Faraday rotation was not used to determine the spontaneous magnetization

Another striking optical property of $LiTbF_4$ is the domain diffraction produced in the ferromagnetic phase. As was discussed in Sec. IV, the ordered phase in $LiTbF_4$ consists of alternate Ising ferromagnetic domains aligned antiparallel. In each domain the population difference in the ground state produces a large zero external-magnetic-field circular birefringence. In the down domains $n_{RCP} >> n_{LCP}$, but in the up domains $n_{LCP} >> n_{RCP}$, and in zero external magnetic field $(n_{LCP} - n_{RCP})_{down} = (n_{RCP} - n_{LCP})_{up}$, where n_{RCP} and n_{LCP} are the indices of refraction for right and left circularly polarized light, respectively. The result of this is that the ferromagnetic domains produce a phase grating, the periodicity of which is determined by the regularity in the size, spacing, and shape of the domains, and the depth of which is determined by the magnitude of $|n_{RCP} - n_{LCP}|$. This is illustrated schematically in Fig. 6.

In the paramagnetic phase in zero external magnetic field, circularly polarized light propagating parallel

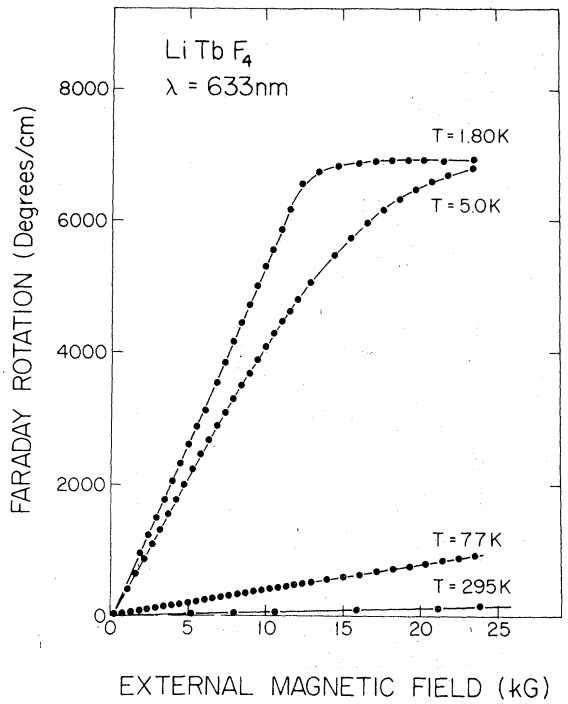

FIG. 5. Faraday rotation vs external magnetic field in $LiTbF_4$ at $T = 295$, 77, 4.2, 1.8 K.

to the c axis passes through the crystal essentially unaffected. In the ferromagnetic phase in zero external magnetic field, this beam encounters a phase grating and part of the transmitted intensity is diffracted into outer lobes.[14] In the presence of an external magnetic field, the phase grating changes. At constant temperature $T \ll T_c$, the application of an external magnetic field parallel to the c axis modifies the fraction of domains that are parallel and antiparallel to the field direction. In a ferromagnet below T_c, the fractions f_p of parallel domains and f_{ap} of antiparallel domains in a field H_{ext} are given by

$$f_p = (1 - f_{ap}) = [1 + H_{ext}/NM_c(T)]/2 , \qquad (11)$$

where N is the demagnetization factor. In the presence of the field, the parallel domains grow in number at the expense of the antiparallel domains, but in each domain the magnetization, and therefore $(n_{RCP} - n_{LCP})$, remains constant. In this case, the phase-grating depth remains constant, but the growth of the parallel domains increases the spacing until the crystal ceases to be a periodic domain structure, which occurs at the paramagnetic phase boundary. As T is increased, the birefringence $(n_{RCP} - n_{LCP})$ for a domain decreases, as a result of the thermal disorder, and at zero magnetic field the depth of the grating is smaller.

This description of $LiTbF_4$ is obviously oversimplified. According to the above description, a periodic diffraction pattern should be observed at $T < T_c$, yet attempts to observe this pattern were unsuccessful. The domains are unlikely to consist of uniformly spaced cylinders as illustrated in Fig. 6. As a result of these simplifications, this model is not quantitatively useful, yet the essential underlying features are borne out by experiment. At $T = 1.5$ K and $H_{ext} = 0$, the forward-direction beam is attenuated by 70% in a crystal 0.4-cm thick at $\lambda = 6328$ Å, where no absorption occurs. This technique of locating the phase boundary by locating the onset of domain diffraction is used in this experiment to map the ferromagnetic-paramagnetic phase boundary.

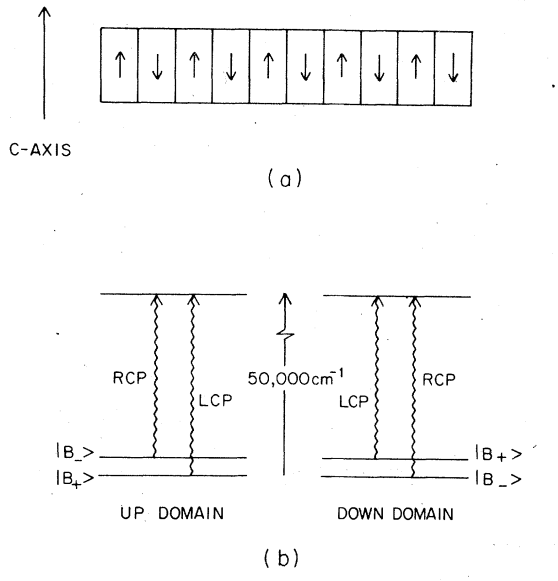

FIG. 6. Part (a) illustrates the uniaxial "cylindrical" ferromagnetic domains in $LiTbF_4$. Part (b) illustrates the optical transition in the two types of domains that are responsible for the phase-grating effect observed in the ordered phase.

Figure 7 illustrates the domain diffraction that occurs on $LiTbF_4$ as the phase boundary is crossed from the paramagnetic to the ferromagnetic phase at $T = 2.6504$ K. The figure illustrates the optical-bridge output (arbitrary units) on the vertical axis as a function of external magnetic field on the horizontal axis. Apart from the spike which occurs upon changing the field, the optical-bridge output remains constant as the external magnetic field is decreased stepwise from 6.505 kG through 6.266 to 6.218 kG. Starting at 6.172 kG, the optical bridge becomes unbalanced, indicating the onset of scattering, and this unbalance increases in amplitude as the field is further decreased to 6.076 kG in Fig. 7. The critical external magnetic field $H_c(T = 2.6504\ \text{K})$ is taken to be 6.195 ± 0.023 kG, the average of 6.218 kG at which no scattering is present, and 6.172 kG, at which scattering definitely is present. By observing the signal-to-noise ratio, it is clear that the value of H_c could be established with a much smaller uncertainty. The reduced temperature t in Fig. 7 is 0.08, and as T_c is approached more closely the scattering becomes harder to detect. In such cases the scans were repeated many times to improve the signal to noise. In all scans it was experimentally verified that the bridge output returned to its balance position when the field was returned to the starting value. The spikes that appear in Fig. 7 are correlated with the rate at which the external field is changed, and may be due to eddy-current heating in the copper sample holder or to a small movement of the sample holder, or possibly to a relaxation occuring in the sample itself.

These types of measurements were made between 1.5 K and T_c and up to 10-kG external magnetic field. Data points at temperatures $T \leq 2.75$ K were obtained from the stepwise external-magnetic-field scans at constant temperature, corresponding to a downward movement across the phase boundary in Fig. 8. In this temperature region the phase boundary was determined to $\pm 0.1\%$ of $M_c(T = 1.5\ \text{K})$. Constant temperature scans from the ferromagnetic to the paramagnetic phase yield the same phase-boundary points. At higher temperatures ($2.85\ \text{K} \leq T \leq T_c$), the phase boundary was obtained by stepwise temperature scans at constant external magnetic field from the paramagnetic to the ferromagnet-

ic phase. As was the case in the field scans, the phase-boundary points obtained showed no hysteresis. In the intermediate temperature range ($2.75 \leq T \leq 2.85$ K), scans of both types were used, and phase-boundary points obtained by field scans were experimentally found to coincide with those obtained by temperature scans. Table I lists the set of external-magnetic-field vs temperature-data points that describe the ferromagnetic-paramagnetic coexistence curve in $LiTbF_4$ obtained from these optical measurements.

VI. ANALYSIS

Table I lists the data pairs that describe the experimentally obtained ferromagnetic-paramagnetic coexistence curve. It is necessary first to transform this data to the temperature dependence of the spontaneous magnetization. In a ferromagnet at temperatures $T \leq T_c$, the magnetization vs external-magnetic-field isotherm is linear in external magnetic field until the ferromagnetic-paramagnetic phase boundary is reached, at which time the magnetization shows little field dependence due to saturation effects. The linear region of the isotherm occurs due to the alignment of the ferromagnetic domains by the external magnetic field, and the slope in this linear region is numerically equal to $1/N$, where N is the sample geometry dependent demagnetization factor. As T is increased toward T_c, the slope of the linear region remains constant, but the critical field $H_c(T)$ required to reach the paramagnetic phase is decreased. In this manner the spontaneous magnetization $M_c(T)$ on the ferromagnetic-paramagnetic phase boundary is related to the critical external magnetic field $H_c(T)$ as shown by

$$H_c(T) = NM_c(T) \ . \tag{12}$$

Using this relation, it becomes clear that a measurement of the coexistence curve in the variables $H_c(T)$ and T is equivalent, apart from the factor $1/N$, to a measurement of the temperature dependence of the spontaneous magnetization. The factor $1/N$ becomes irrelevant when the magnetization is normalized by the saturation magnetization

$$M_c(T=0) = (1/N)H_c(T=0) \ ,$$

so that we obtain

$$M_c(T)/M_c(0) = H_c(T)/H_c(0) \ . \tag{13}$$

Using this relation, the data in Table I is transformed into the temperature dependence of the reduced spontaneous magnetization, and this data is plotted in Fig. 8 between 1.5 K and T_c, using

$$H_c(T=1.5 \text{ K}) = 0.93 H_c(T=0)$$

and

$$H_c(T=1.5 \text{ K}) = 9.301 \text{ kG} \ .$$

The error bars on Fig. 8 reflect the uncertainty in locating the onset of domain scattering, and are considerably smaller than those obtained by isothermal-magnetization vs external-magnetic-field measurements.

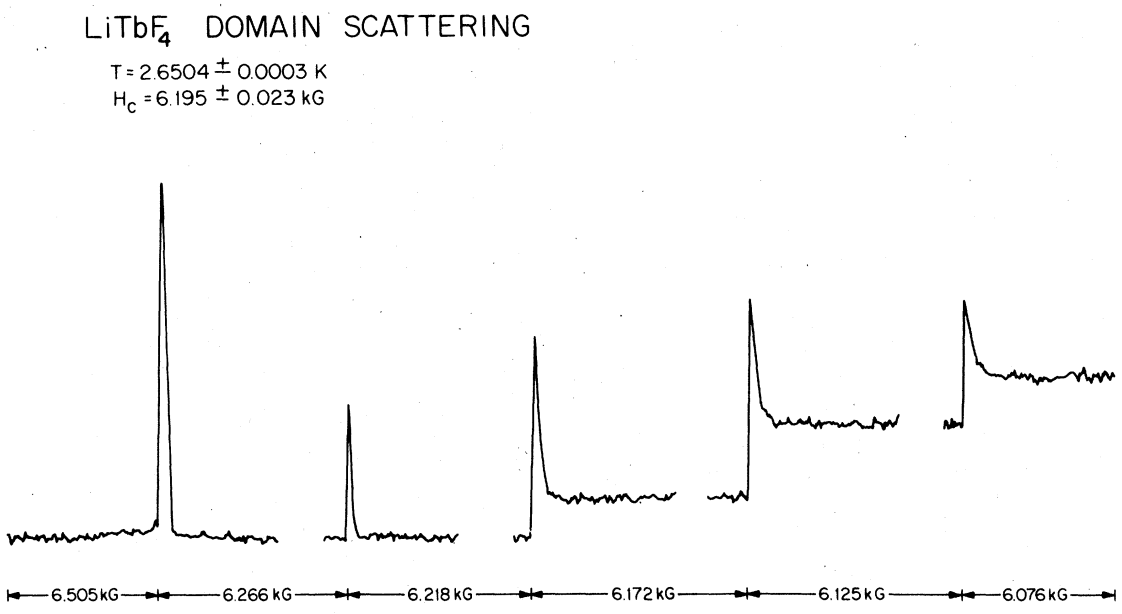

FIG. 7. Data illustrating optical-bridge unbalance due to domain diffraction in the ferromagnetic phase.

The data in Table I and Fig. 8 were quantitatively compared to three relations that could be used to describe the temperature dependence of the spontaneous magnetization near T_c. According to the renormalization-group treatment this is given by

$$M_c(T)/M_c(0) = B|t|^{1/2}|\ln|t_0/t|\,|^{1/3}\,, \tag{14}$$

where t_0 represents the effect of higher-order logarithmic corrections. An alternative possibility is the more common power law

$$M_c(T)/M_c(0) = B|t|^{\beta}\,. \tag{15}$$

A final, although unlikely, possibility is the mean-field power law without logarithmic corrections

$$M_c(T)/M_c(0) = B|t|^{1/2}\,. \tag{16}$$

The data were fit to each of these relations using a nonlinear least-squares program, and the results of this analysis is quantitatively summarized in Table II. For each of the three relations Table II illustrates the range of reduced temperature used in the fit, the resultant χ^2, and the best-fit coefficients. In Table II the uncertainties quoted represent approximately a doubling of χ^2. The fit to the mean-field theory, relation (16) is seen to result in coefficients B and T_c that are quite sensitive to the range in reduced temperature t and also yields a value of χ^2 which is relatively large. Equation (16) is ruled out, as would be expected. The fit to Eq. (15) is also summarized in Table II. This fit provides an effective exponent β. In Table II the results of the fit of our data to Eq. (15) indicate that $0.81 \leq \chi^2 \leq 2.3$, that $2.8668 \leq T_c \leq 2.8686$ K, that $1.6 \leq B \leq 1.7$, and $0.36 \leq \beta \leq 0.39$, depending on the range of reduced temperature t used in the fit. We cannot definitely rule out Eq. (15) as a possible description of the observed behavior. Finally, the results of fitting our data to Eq. (14) also appear in Table II. In this fit, we find that $0.52 \leq \chi^2 \leq 0.54$, that $2.8700 \leq T_c \leq 2.8702$ K, that $1.77 \leq B \leq 1.79$, and that $0.52 \leq t_0 \leq 0.57$, depending on the range in reduced temperature t that

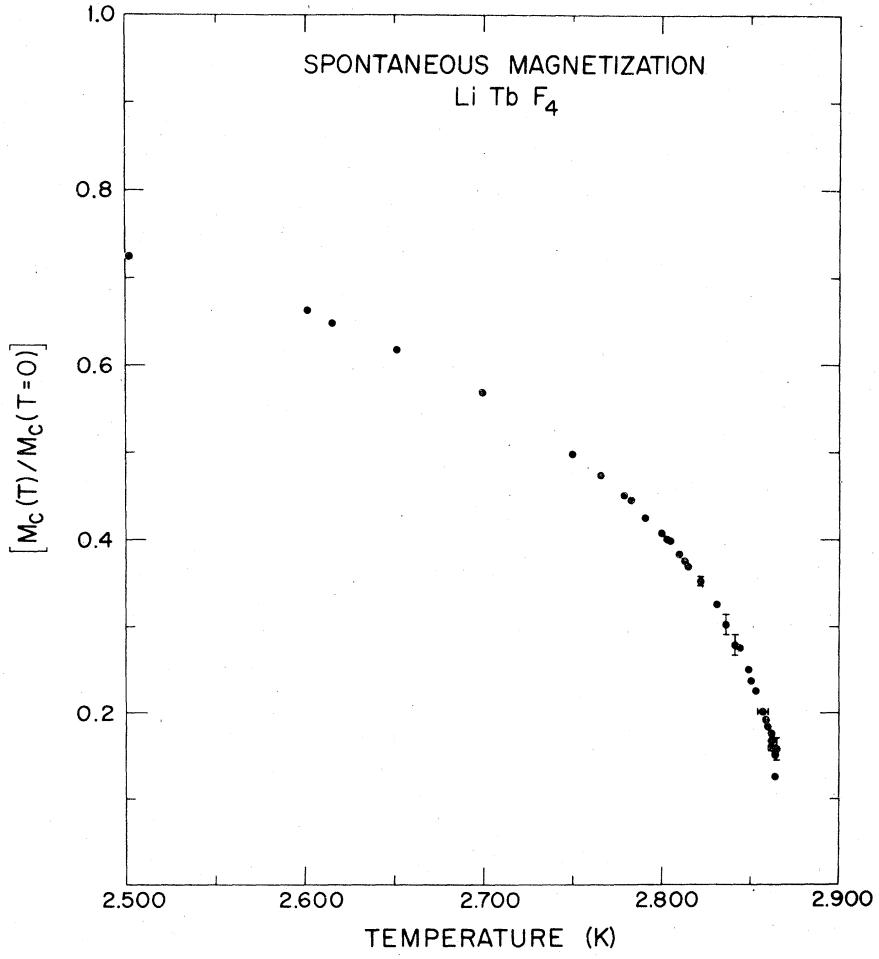

FIG. 8. Phase diagram of normalized spontaneous magnetization $M_c(T)/M_c(0)$ vs temperature obtained from the data in Table I.

TABLE II. Parameters and equations (see text for details) used to fit saturation magnetization data for $LiTbF_4$.

Eq. Used in Fit	t	B	T_c (K)			χ^2
	$0.002 \leq t \leq 0.04$	1.79 ± 0.02	2.8700 ± 0.002		0.524 ± 0.047	0.54
(14)	$0.002 \leq t \leq 0.06$	1.78 ± 0.04	2.8702 ± 0.002	t_0	0.553 ± 0.036	0.52
	$0.002 \leq t \leq 0.09$	1.77 ± 0.06	2.8702 ± 0.002		0.568 ± 0.014	0.54
	$0.007 \leq t \leq 0.06$	2.33 ± 0.024	2.885 ± 0.008		...	12.4
(16)	$0.013 \leq t \leq 0.10$	2.13 ± 0.201	2.902 ± 0.010		...	51.2
	$0.001 \leq t \leq 0.04$	1.71 ± 0.02	2.8686 ± 0.0032		0.385 ± 0.003	0.81
(15)	$0.001 \leq t \leq 0.06$	1.66 ± 0.01	2.8680 ± 0.0032	β	0.377 ± 0.002	0.92
	$0.0009 \leq t \leq 0.09$	1.55 ± 0.01	2.8668 ± 0.0034		0.357 ± 0.001	2.26

(14) $M_c(T)/M_c(0) = B|t|^{1/2}|\ln|t_0/t|\,|^{1/3}$

(16) $M_c(T)/M_c(0) = B|t|^{1/2}$

(15) $M_c(T)/M_c(0) = B|t|^{\beta}$

is selected. Equation (14) fits our data with a χ^2 that is not only smaller than that obtained using Eq. (15), but which is also changing by only ~4% over the range in t which produced a change of ~300% in χ^2 using relation (15). Our fit to Eq. (14) indicates that the observed behavior of the spontaneous magnetization and the predicted logarithmic corrections to a mean-field-theory (MFT) power law are quantitatively consistent, that the χ^2 of the fit obtained is insensitive to the range of t selected, and that the coefficients in the fit are also quite insensitive to the range of t. None of these features occurred in the fit to Eq. (15). The parameter t_0 obtained from (14) is $t_0 = 0.53 \pm 0.06$. Figures 9, 10, and 11 illustrate the best fits to each of these three relations using the parameters listed in Table II.

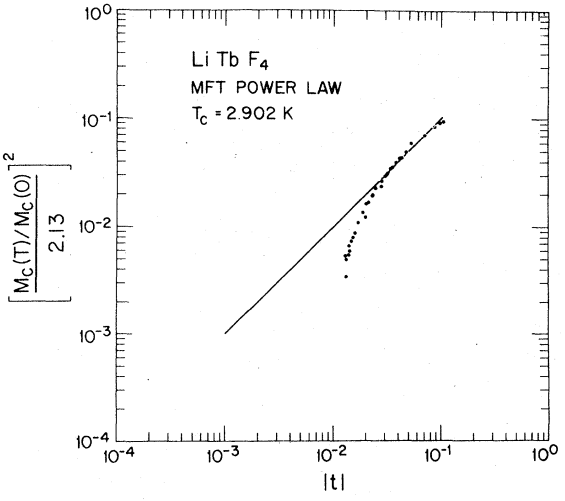

FIG. 9. Figure of best fit of MFT power law, Eq. (16), to temperature dependence of the spontaneous magnetization.

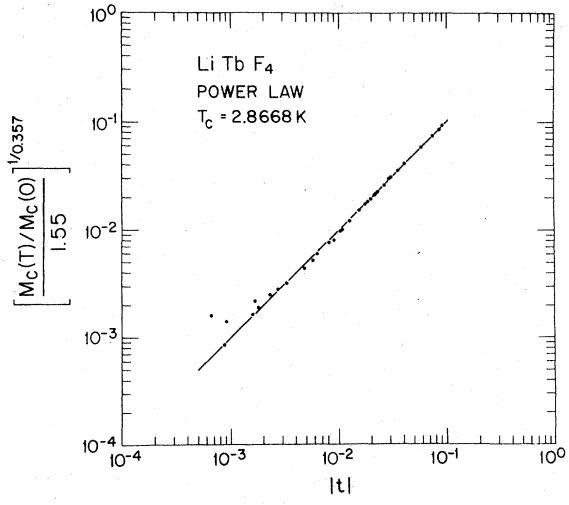

FIG. 10. Figure of best fit of power law, Eq. (15), to the temperature dependence of the spontaneous magnetization.

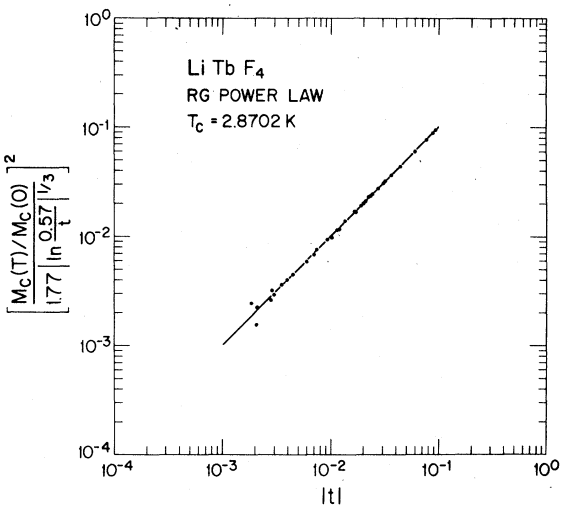

FIG. 11. Figure of best fit of renormalization-group (RG) power law, Eq. (14), to the temperature dependence of the spontaneous magnetization

VII. COMPARISON WITH OTHER EXPERIMENTS, AND CONCLUSIONS

As we pointed out in Sec. II, it is of special interest to test the renormalization-group results at the upper marginal dimensionality. Since $d^* = 3$ for tricritical points and for dipolar Ising ferromagnets, these are systems convenient for such a test. Experimental studies of various tricritical points[15] confirm that a mean-field description is valid, which is consistent with the renormalization-group (RG) prediction.[5] However, the data show no sign of the expected logarithmic corrections. For a dipole Ising ferromagnet, these logarithmic corrections are quite prominent and lead to effective exponents (when power-law behavior is assumed) quite different from the mean-field values. Tricritical-point experiments differ because the theoretical scaling fields and densities are not the ones experimentally accessible, but we do not understand why the effect of logarithmic corrections has not been observed.

The validity of theoretical predictions is more firmly established for dipolar Ising ferromagnets. The critical equation of state for dysprosium ethyl sulphate has been measured[16] and found to agree with theoretical predictions.[6–8] Although simple power laws were found to represent the data as well as classical results with logarithmic corrections, the relation among critical amplitudes that was predicted for the latter representation was experimentally confirmed; this provides a confirmation of RG calculations. There have been several tests of RG theory for $LiTbF_4$. The specific-heat $|\ln|t||^{1/3}$ prediction has been observed,[17] and the relation of Eq. (9) has also been verified.[18] While neutron-scattering measurements of the magnetization[19] were not sufficiently precise to confirm Eq. (6), the results presented in this paper do so. Thus most of the RG predictions for $LiTbF_4$ appear to be verified; it remains to carry out precision measurements of the magnetic equation of state.

ACKNOWLEDGMENTS

We wish to thank D. Gabbe and A. Linz for growing the crystal of $LiTbF_4$. D. E. Cooper provided valuable assistance in making some of the measurements and we enjoyed stimulating discussions with J. Als-Nielsen. This work was performed at the National Magnet Laboratory and supported by NSF Grant Nos. DMR-76-80895 and MRL-DMR-76-80994.

APPENDIX

As explained above, the measurements presented here consist of a determination of the external magnetic field and temperature dependence of the onset of domain diffraction. This onset of diffraction is used as an optical indication of the location of the paramagnetic-ferromagnetic coexistence curve. In order to make precision measurements of this phase boundary, a two-beam optical-bridge system was utilized.

Figure 1 illustrates, schematically, the optical system. The 1-mW beam from a He-Ne alignment laser with $\lambda = 6328$ Å is first attenuated by a factor 10 by the neutral density filter ND; next, it passes through a linear polarizer $P_1(0°)$ oriented at 0°, next through a Morvue photoelastic modulator MB(45°) oriented at 45°, and next through a beam splitter BS. The lower beam, the sample beam in Fig. 1, passes next through another linear polarizer P_2 (0°), a circular polarizer CP_1, the $LiTbF_4$ crystal which is mounted in a cryostat between the pole faces of an electromagnet, and finally into a RCA7265 photomultiplier tube. The upper beam, the reference beam, passes from the beam splitter to mirror M_1, through a linear polarizer $P_3(90°)$, a circular polarizer CP_2 a reference attenuator, another pair of mirrors M_2 and M_3, and finally into the same photomultiplier tube.

The operation of this optical bridge is based on the photoelastic modulator. The photoelastic modulator consists of a fused-quartz block oscillating at a frequency of $\omega/2\pi = 50$ kHz. The oscillations produce a strain at this frequency that, in turn, produces a modulation of the index of refraction parallel to the oscillation axis. The resultant birefringence $\delta(t)$ is given by

$$\delta(t) = A\cos\omega t\ ,$$

where A is the amplitude of the birefringence oscillation. If light is passed first through a linear polarizer $P_1(0°)$ oriented at 0°, next through the photoelastic modulator MB(δ, 45°), next through another linear polarizer $P_2(\beta)$ oriented at an angle β, and finally

into the photomultiplier tube, then the intensity at the photomultiplier tube is given by

$$I(\beta) = I_0[1 + \cos(2\beta)\cos\delta] ,$$

where I_0 is the incident laser intensity, β is the angle of the second polarizer $P_2(\beta)$ with respect to the first polarizer $P_1(0°)$, and δ is the birefringence modulation produced by the photoelastic modulator bar. Using

$$\cos(A\cos\omega t) = J_0(A) + 2J_2(A)\cos 2\omega t + \cdots ,$$

where $J_0, J_2 \cdots$ are Bessel functions of even order, the intensity component at frequencies 2ω and at dc ($\omega = 0$) are

$$I_{2\omega}(\beta) = I_0[2J_2(A)\cos(2\beta)] ,$$

$$I_{dc}(\beta) = I_0[1 + J_0(A)\cos(2\beta)] .$$

If $2\beta = 0$, then $I_{2\omega} = 2J_2(A)I_0$; but if $2\beta = \pi$, then $I_{2\omega} = -2J_2(A)I_0$, and this feature is responsible for the operation of the optical bridge. In the sample beam $P_2(2\beta) = P_2(2\beta = 0°)$, and in the reference beam $P_3(2\beta) = P_3(2\beta = \pi)$. In this configuration, the total intensity at the photomultiplier tube is

$$I_{2\omega}^{\text{total}} = I_0(T^S - T^R)2J_2(A_0) ,$$

$$I_{dc}^{\text{total}} = I_0(T^S + T^R) ,$$

where the depolarization effects of the mirrors M_1, M_2, M_3, and of the BS have been neglected, where $(T^S)^{1/2}$ and $(T^R)^{1/2}$ are the transmission of the sample and the reference attenuator, and where the modulation amplitude has been adjusted to $A_0 = 108°$ so that $J_0(A_0) = 0$. In this method the 2ω component of the intensity striking the photomultiplier tube is proportional to the difference in transmission between the crystal and the reference-beam attenuator, and the incident-laser intensity I_0. A dc photomultiplier feedback circuit is used to maintain the dc phototube anode current constant by varying the gain of the phototube. Using this technique, the dc signal from the phototube S_{dc} is held constant so that we have

$$S_{dc} = gI_0(T^S + T^R) = \text{constant} \equiv S_0 ,$$

$$S_{2\omega} = gI_0(T^S - T^R)2J_2(A) ,$$

where g is the phototube gain. In this manner the 2ω signal from the phototube is given by

$$S_{2\omega} = S_0 \frac{T^S - T^R}{T^S + T^R} 2J_2(A_0) ,$$

and this provides an electrical signal proportional only to the difference in transmissions of the two beams. The depolarization produced by the beam splitter and the mirrors produces a reduction in overall sensitivity, but at constant wavelength this reduction remains constant and does not affect the determination of the phase boundary. The circular polarizers are inserted to eliminate Faraday rotation by the sample. The variable attenuator was constructed by placing a linear polarizer after $P_3(90°)$ on a precision rotary stage. All polarizers were Polaroid HN-22. The primary limitation to this technique is the time stability of the null. In a typical twenty-minute interval, the stability obtained was equivalent to a 0.1% change in T^S.

[1] V. L. Ginzburg, Sov. Phys. Solid State 2, 1824 (1960).

[2] J. Als-Nielsen and R. J. Birgeneau, Am. J. Phys. 45, 554 (1977).

[3] K. G. Wilson and J. Kogut, Phys. Rev. C 12, 75 (1974); M. E. Fisher, Rev. Mod. Phys. 46, 597 (1974); S. K. Ma, *ibid.* 45, 589 (1973); S. K. Ma, *Modern Theory of Critical Phenomena* (Benjamin, New York, 1976); P. Pfeuty and G. Toulouse, *Introduction to the Renormalization Group and to Critical Phenomena* (Wiley, New York, 1977).

[4] E. Brezin, J. C. LeGuillon, and J. Zinn-Justin, Phys. Rev. D 9, 1121 (1974).

[5] F. J. Wegner and E. H. Riedel, Phys. Rev. B 7, 248 (1973).

[6] A. Aharony and M. E. Fisher, Phys. Rev. B 8, 3323 (1973); A. Aharony, Phys. Rev. B 8, 3342 (1973); 8, 3349 (1973); 8, 3358 (1973); 8, 3363 (1973).

[7] A. Aharony and B. I. Halperin, Phys. Rev. Lett. 35, 1308 (1975).

[8] A. I. Larkin and D. E. Khmel'nitskii, Zh. Eksp. Teor. Fiz. 56, 2087 (1969) [Sov. Phys. JETP 29, 1123 (1969)].

[9] D. Gabbe and A. L. Harmer, J. Crystal Growth 3, 4 (1968).

[10] L. M. Holmes, T. Johansson, and H. J. Guggenheim, Solid State Commun. 12, 993 (1973); L. M. Holmes, H. J. Guggenheim, and J. Als-Nielsen, *Tr. Mezhdunar Konf. Magn. 1973* (Nauka, Moscow, 1974), Vol. 6, p. 256.; L. M. Holmes, J. Als-Nielsen, and H. J. Guggenheim, Phys. Rev. B 12, 180 (1975).

[11] P. E. Hansen, T. Johansson, and R. Nevald, Phys. Rev. B 12, 5315 (1975).

[12] J. A. Griffin, J. Folkins, M. J. Weber, R. Morgret, D. Gabbe, and A. Linz, J. Appl. Phys. 49, 2209 (1978); M. J. Weber, R. Morgret, S. Y. Leung. J. A. Griffin, D. Gabbe, and A. Linz (unpublished).

[13] The samples used in Figs. 5 and 8 have different demagnetization factors, and therefore $H_c(T)$ in Fig. 5 differs from Fig. 8.

[14] Diffraction by magnetic domains occurs in many other materials. See, for example, J. F. Dillon, Jr., E. Yi Chen, H. J. Guggenheim, and Richard Alben, Phys. Rev. B 15, 1422 (1977); J. A. Griffin, S. E. Schnatterly, Y. Farge, M. Regis, and M. P. Fontana, Phys. Rev. B 10, 1960 (1974); J. F. Dillon, Jr., and J. P. Remeika, J. Appl. Phys. 34, 637 (1963); and J. C. Suits, J. Appl. Phys. 38, 1498 (1967).

[15] J. A. Griffin and S. E. Schnatterly, Phys. Rev. Lett. 33, 1576 (1974); R. J. Birgeneau, G. Shirane, M. Blume, and

W. C. Koehler, Phys. Rev. Lett. 33, 1098 (1974); P. Leiderer, D. R. Watts, and W. W. Webb, Phys. Rev. Lett. 33, 483 (1974); G. Ahlers and D. S. Greywall, Phys. Rev. Lett. 29, 849 (1972).

[16]R. Frowein and J. Kötzler, A. Phys. B 25, 279 (1976).

[17]G. Ahlers, A. Kornblit, and H. J. Guggenheim, Phys. Rev. Lett. 34, 1227 (1975).

[18]J. Als-Nielsen, Phys. Rev. Lett. 37, 1161 (1976).

[19]J. Als-Nielsen, L. M. Holmes, F. Krebs Larsen, and H. J. Guggenheim, Phys. Rev. B 12, 191 (1975).